PCCP

ARTICLE TYPE

Cite this: DOI: 00.0000/xxxxxxxxxx

3-methylation alters excited state decay in photoionised uracil

Javier Segarra-Martí,*[a] Thierry Tran,[b,c] and Michael J. Bearpark*[b]

Received Date
Accepted Date

DOI: 00.0000/xxxxxxxxxx

UV and VUV-induced processes in DNA/RNA nucleobases are central to understand photo-damaging and photo-protecting mechanisms in our genetic material. Here we model the events following photoionisation and electronic excitation in uracil, methylated in the 1' and 3' positions, using the correlated XMS-CASPT2 method. We compare our results against those for uracil and 5-methyl-uracil (thymine) previously published. We find 3-methylation, an epigenetic modification in non-negligible amounts, shows the largest differences in photoionised decay of all three derivatives studied compared to uracil itself.At the S_0 minimum, 3-methyl-uracil (3mUra) shows almost degenerate excited cation states. Upon populating the cation manifold, a crossing is predicted featuring different topography compared to other methylated uracil species in this study. We find an effective 3-state conical intersection accessible for $3mUra^+$, which points at an additional pathway for radiationless decay. 3-methylation reduces the potential energy barrier mediating decay to the cation ground state, making it vanish and leading to a pathway that we expect will contribute to the fastest radiationless decay amongst all methylated uracil species studied to date. 1- and 5-methylation, on the other hand, give differences from uracil in detail only: ionisation potentials are slightly red-shifted and the potential energy barrier mediating decay to the cation ground state is small but almost unchanged. By comparing against CASSCF calculations, we establish XMS-CASPT2 is essential to correctly describe conical intersections for $3mUra^+$. Our calculations show how a chemical modification that seems relatively small electronically can nevertheless have a significant impact on the behaviour of electronic excited states: a single methylation in the 3' position alters the behaviour of the RNA base uracil and appears to open an additional pathway for radiationless decay following ionisation and electronic excitation.

1 Introduction

Radiation induced phenomena in the DNA/RNA chromophoric species the nucleobases[1–4] is a topic within physical chemistry with deep implications for healthcare concerns such as skin cancer melanoma.[5,6]

DNA/RNA absorb radiation efficiently in the UV range. The extra energy gained upon absorption can be released harmlessly through ultrafast excited state decay processes which underpin the photo-protection mechanisms of our genetic material,[3,4] but such energies can also trigger chemical reactions leading to photo-products (lesions) that compromise the integrity of our genetic code.[1,5]

Methylation strongly affects the photoinduced properties of the nucleobases.[7–10] Previous experimental and theoretical work has shown increased excited state lifetimes and thus the likelihood of further reactions with neighbouring species, which could enhance DNA damage.[11] Recent studies show over 40% of tumours formed in melanomas are related to C5-methylation.[12]

Beyond 5-methylation, which refers to the well-known canonical DNA nucleobase thymine,[13] other instances are found in our genetic code to a lesser extent. Among these, 3-methyl-uracil has recently attracted attention as it is a potential epigenetic modification of the RNA nucleobase uracil.[14] Epigenetic modifications refer to heritable changes made to DNA/RNA sequences that regulate how genes are expressed but that do not affect the nucleotide sequence itself, chemical modification in the form of methylation being one of the main substitutions with 5-methyl-cytosine the most prominent case.[15] 1-methyl-uracil, on the other

[a] Instituto de Ciencia Molecular, Universitat de Valencia, P.O. Box 22085, ES-46071 Valencia, Spain; E-mail: javier.segarra@uv.es
[b] Department of Chemistry, Molecular Sciences Research Hub, Imperial College London, White City Campus, 82 Wood Lane, W12 0BZ, London, UK; E-mail: m.bearpark@imperial.ac.uk
[c] Université de Nantes, CNRS, CEISAM UMR 6230, F-44000 Nantes, France.

† Electronic Supplementary Information (ESI) available: Cartesian coordinates of all critical structures, ionisation potential values for the different CASPT2 Hamiltonians and conical intersection parameters at the CASSCF level of theory. See DOI: 10.1039/cXCP00000x/

hand, is an important derivative often studied experimentally[7] due to its improved solubility and induced spectral shifts that resemble those of natural substitutions in position 1' such as sugars and phosphates.

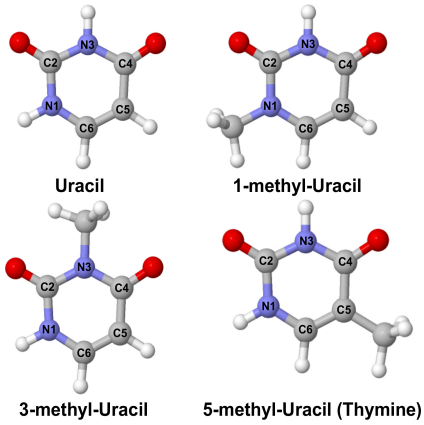

Fig. 1 The different methylated uracil species studied in this work with their atom labelling: uracil (Ura), 1-methyl-uracil (1mUra), 3-methyl-uracil (3mUra) and 5-methyl-uracil (5mUra or thymine).

DNA photoionisation has been studied less than photoexcitation, and even less in the context of methyl-substituted and other non-canonical DNA/RNA species. This is partly due to their high ionisation energies, placed in the Vacuum UV (VUV, ∼8 eV) range,[16–23] which is mostly filtered by the ozone layer and thus not considered as directly relevant to sunlight damage.[24]

Two recent advances, however, have rekindled the interest of the community in DNA photoionisation. Experiments have recorded sizeable cation yields in double-helix DNA structures when excited with 266 nm wavelengths well below their ionisation potential.[25–27] This ongoing puzzle points to hidden mechanisms promoting cation (doublet state) formation in DNA systems at lower energies than previously thought,[25] which implies a potential role for cations also in UV-driven photo-processes such as those mediated by charge separated states.[28–30] Additionally, new light sources are emerging with sufficiently high energies and intensities to monitor photoionisation processes experimentally.[31,32] With sufficient spectral and temporal resolution these offer a way to study the intrinsic properties of cationic species systematically[33,34] in the gas phase.

In this work we model the 1- and 3-methylated uracil species shown in Fig. 1 and compare them against previously studied uracil and thymine.[17] Fig. 2 summarises the decay processes in these systems following vertical ionisation and electronic excitation.

We observe the largest substitution effects for the 3-methylated species, which features almost degenerate cation electronic excited states at the S_0 minimum geometry (Section 3.1). Accessing either of the excited cation states leads to a nearby $^2\pi^+_{H-1}/^2n^+_O$ conical intersection (Section 3.2) that features a different topography compared to all other systems studied (Section 3.3). Moreover, a small (< 0.2 eV) energy gap is observed between this intersection and the cation ground state (left inset in Fig. 2), and further optimisation leads to an effective 3-state intersection with potential to enable direct $^2\pi^+_{H-1} \rightarrow {}^2\pi^+_H$ population transfer to the cation ground state.[35,36] Further evolution leads to a shallow $^2n^+_O$ state minimum connected barrierlessly to an $^2n^+_O/^2\pi^+_H$ intersection which mediates decay to the cation ground state (right inset in Fig. 2). We thus predict the 3-methylated species to feature the fastest decay amongst all methylated uracil species compared and studied here.

Methylation modulates the energy gap between the $(^2\pi^+_{H-1}/^2n^+_O)_{CI}$ crossing and the $^2\pi^+_H$ cation ground state: the unmethylated species shows the largest gap[17] while the different substitutions decrease this energy difference. The position in which the methyl group is added also affects the small energy barrier mediating decay to $^2\pi^+_H$.

Our work discerns subtle but important changes in the cationic excited state manifold of DNA/RNA nucleobases upon methylation - the most common epigenetic modification in our genetic material - which alters their photoionised decay.

2 Computational Details

CASSCF wave functions were averaged over five doublet states and were subsequently used for single-point CASPT2 energy corrections.[37–39] An analogous active space was used for all species, which comprised the full π valence occupied and virtual space plus the two occupied n_O lone pairs, totalling 14 electrons in 10 orbitals for the neutral and 13 electrons in 10 orbitals for the cationic species. An imaginary level shift of 0.2 a.u. was employed in the perturbative step to avoid the presence of intruder states,[40] and IPEA shifts[41] of 0.0 and 0.25 a.u. were tested as this correction has been shown to improve the description of cationic open-shell states in these systems.[16]

For computing the ionisation potentials, CASPT2 calculations were carried out with single-state,[37–39] multistate (MS),[42] and extended multistate (XMS)[43] variants to benchmark the effect of the zeroth order Hamiltonian on the cationic manifold, using the OpenMolcas software.[44,45] For presenting and discussing the energies in the Franck-Condon (FC) region (S_0 minimum) we averaged over the different CASPT2 formulations.[17] However, for geometries and energies away from equilibrium we report only XMS-CASPT2(IPEA=0.0) estimates as they were found to provide a better balance for the simultaneous description of covalent and ionic excited states[43] and give more reliable estimates close to or at crossing regions.[46,47]

Ground and excited state optimisations were carried out with BAGEL.[48,49] Correlation consistent cc-pVDZ basis set and its density fitting auxiliary basis was used throughout.[50] The characterised cationic ground and excited state minima, as well as low-lying conical intersections (CIs), were optimised at the XMS-CASPT2 level of theory as dynamic electron correlation has previously been shown to be important for the description of DNA-based systems.[9,51–54] XMS-CASPT2 minima and CI optimisations (with the projection method[55]) used implementations of analytic gradients[56–59] and couplings.[60,61] We ran linear interpolations in internal coordinates between the different critical structures optimised to ensure no energy barriers were present; we have connected energetically the critical structures but not included these interpolated points as they offered no extra value. An ef-

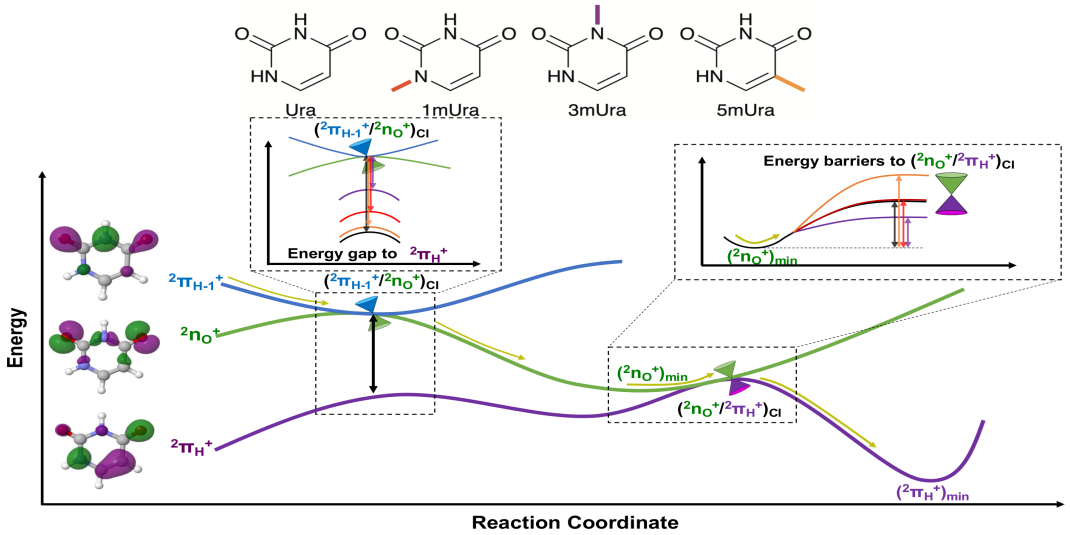

Fig. 2 Overview of the photoionised decay process in the different systems compared here and the distinct electronic states that take part: $^2\pi_H^+$ in purple, $^2n_O^+$ in green and $^2\pi_{H-1}^+$ in blue. Two insets are provided which highlight the main differences observed across systems: the energy gaps between $(^2\pi_{H-1}^+/^2n_O^+)_{CI}$ and $^2\pi_H^+$ and the energy barriers to access $(^2n_O^+/^2\pi_H^+)_{CI}$ mediating decay to the cation ground state. Energy gaps/barriers are denoted in different colours for the different species: black for uracil (Ura), red for 1-methyl-uracil (1mUra), purple for 3-methyl-uracil (3mUra) and orange for 5-methyl-uracil (5mUra).

fective 3-state conical intersection[62,63] was located in 3mUra$^+$; this was done by optimising the intersection between $^2\pi_{H-1}^+$ and $^2\pi_H^+$ states, i.e. energetically the first and third cation electronic states, leading to an effective $^2\pi_{H-1}^+/^2n_O^+/^2\pi_H^+$ degeneracy.

Conical intersection parameters were extracted from XMS-CASPT2 gradient difference and non-adiabatic coupling vectors obtained at minimum energy crossing points.[64] These vectors were used to obtain pitch (δ), asymmetry (Δ) and relative tilt (σ), as well as the $\mathscr{P}$ and $\mathscr{B}$ parameters defining intersection types.[65] We choose branching plane vectors so that $\Delta \geq 0$ and $\theta_s \in [0, \frac{\pi}{2}]$, to make them comparable.[65]

3 Results

We start by comparing new calculations for 1- and 3-methylated species to our previously published estimates for uracil and thymine,[17] first showing how methylation affects the energies of the doublet (cationic) state manifold (i.e. ionisation potentials, Section 3.1). We then show how methylation affects the cationic excited state decay process (Section 3.2), before analysing how methylation (Section 3.3) and dynamic electron correlation (Section 3.4) affect the conical intersection topographies in these systems.

3.1 Ionisation potentials

Fig. 3 shows the spread of computed vertical ionisation potentials of methylated uracil species, compared to literature experimental values for uracil and thymine,[19,21,22] and for 1-methyl-uracil.[66] (There are currently no experimental values for 3-methyl-uracil). Values discussed below in this section are the CASPT2 average values (black crosses in Fig. 3) unless otherwise stated explicitly.

Looking across the four different panels in Fig. 3 shows how the SOMOs characterising the cationic states are largely unaffected upon methylation, making the electronic states considered here directly comparable across the different systems studied.

The first ionisation potential for all methylated systems corresponds to the $^2\pi_H^+$ state, depicted as purple boxes in Fig. 3. The average CASPT2 value for uracil itself is around 9.5 eV[17] in excellent agreement with experiment,[19,21,22] with a relatively small energy spread across the different zeroth-order Hamiltonians. In contrast, 1-methyl-uracil (1mUra, Fig. 3b) displays the largest spread of calculated energy values for this state (almost 1 eV), which makes it difficult to assess whether this methylation red-shifts or blue-shifts the first ionisation potential with respect to Ura. Furthermore, the slightly lower calculated value of 9.42 eV is ~0.3 eV higher than the experimental evidence available,[66] which is the largest such difference from experiment found in this study. 3mUra and 5mUra both appear to red-shift the first ionisation potential with respect to Ura: their calculated ionisation potentials are placed at 9.30 and 9.22 eV, respectively; the latter agreeing to around a tenth of an eV with the available experimental evidence at ~9.1 eV.[19,21,22]

The second ionisation potential in Ura (green box in Fig. 3a) corresponds to the $^2n_O^+$ electronic state. Its average CASPT2 value at 10.00 eV is around a tenth of an eV from the experimental ~10.08 eV.[19,21,22] Upon 1-methylation, Fig. 3b shows a large increase in the spread of energy values associated with this transition while the average hardly changes at 10.05 eV.

3-methylation, however, most noticeably produces a much larger shift for the $^2\pi_{H-1}^+$ state. As Fig. 3c shows, this creates a near degeneracy between the $^2n_O^+$ and $^2\pi_{H-1}^+$ states in the Franck-Condon (FC) equilibrium region. The CASPT2-averaged values for $^2n_O^+$ and $^2\pi_{H-1}^+$ are 9.63 and 9.81 eV, respectively: a small red shift in the ionisation potential of the $^2n_O^+$ state (~0.3 eV) but a more pronounced one for the $^2\pi_{H-1}^+$ state of ~0.7 eV with respect to Ura.

These changes induced upon 3-methylation are understandably

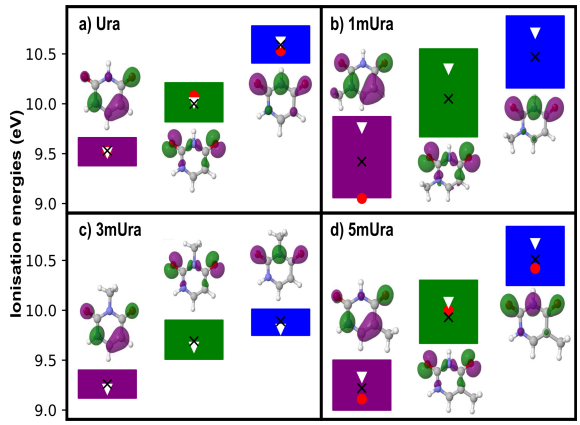

Fig. 3 Schematic representation of the gas phase vertical (at FC, the S_0 minimum) ionisation potentials of a) uracil (Ura),[17] b) 1-methyl-uracil (1mUra), c) 3-methyl-uracil (3mUra) and d) 5-methyl-uracil (5mUra, thymine).[17] Purple denotes the ionisation energy ranges for $^2\pi_H^+$, green for $^2n_O^+$, and blue for $^2\pi_{H-1}^+$ states. The energy range spanned by the different zeroth-order Hamiltonians is shown by boxes; their specific values are given in Tables S1 and S2 of the SI for 1mUra and 3mUra and in the literature for Ura and 5mUra.[17] CASPT2 average values are represented by black crosses, XMS-CASPT2(IPEA=0.0) values (used later in Section 3.2) are given by white inverted triangles, while red dots denote the available experimental evidence for Ura/5mUra[19,21,22] and 1mUra.[66] The singly occupied molecular orbitals (SOMOs) that define the different cationic states are also shown.

the most significant: Fig. 3c shows that the additional methyl group is introduced in the part of the molecular frame where SOMO is localised.

5mUra, on the other hand, was found to produce a small red-shift to the $^2n_O^+$ ionisation potential[17] in agreement with the available experimental evidence and in line with the calculations presented here for 1mUra.

The third and last ionisation potential considered here is that of the $^2\pi_{H-1}^+$ state, which is calculated to be 10.59 eV for Ura (Fig. 3a), in agreement with the recorded evidence at ∼10.53 eV. Methylation in the 1' position red-shifts the average CASPT2 value to 10.47 eV, within a tenth of an eV of Ura, while methylation in the 3' position leads to the more pronounced ∼0.7 eV red-shift discussed above. 5'-methylation produces a small red-shift in the ionsation energy of the $^2\pi_{H-1}^+$ state[17], in agreement with the 1' substituted species.

In this work we chose to look for three cation states. For 3mUra$^+$, the next cation state is ∼1 eV higher in energy, and for now we make the assumption that this and other upper excited states will decay to these three lower states via radiationless channels for future study. Our focus here is to understand the lower excited states, and in particular any barriers or factors that might influence radiationless decay to the cation ground state.

Overall, methylation leads to a stabilisation of the cationic electronic state manifold. This is expected when introducing an electron donor group such as methyl into an organic cationic species, and is reflected to varying degrees across the different substitutions. 1-methylation values are comparable to those previously calculated for 5mUra (thymine),[17] but with a larger spread of energy values across the different CASPT2 formulations. 3-methylation, on the other hand, shows almost degenerate $^2n_O^+$ and $^2\pi_{H-1}^+$ states at the FC / S_0 minimum geometry: both $^2n_O^+$ and $^2\pi_{H-1}^+$ states appear strongly red-shifted with respect to Ura, as methylation occurs right onto the molecular frame where the SOMOs defining these cationic states are localised.

These results also serve to calibrate the different CASPT2 formulations for describing potential energy hypersurfaces in the cationic state manifold for DNA/RNA pyrimidine derivatives. We chose XMS-CASPT2(IPEA=0.0) for the geometry optimisations reported in Sections 3.2 for the following reasons: as shown in Fig. 3 (white inverted triangles) this method shows overall good agreement with the available experimental evidence except for the $^2\pi_H^+$ state in 1mUra, and XMS-CASPT2 is also preferred for describing correctly potential energy crossings and nearby regions.[46]

3.2 Excited state evolution

Strong fields are predicted to ionise electrons from different molecular orbitals with very similar probabilities,[67] leading to multiple states.[35,67–71] As the initial ionised state cannot then be easily assigned, we assume here initial population of the $^2\pi_{H-1}^+$ state and all critical molecular structures (i.e. ground and excited state minima, as well as conical intersections) are characterised between this state and all lower-energy doublets until reaching the cationic $^2\pi_H^+$ ground state.[17,18]

Fig. 4 shows the potential energy surfaces computed for a) 1mUra$^+$ and b) 3mUra$^+$ compared to Ura$^+$[17] (shaded lines) as a reference. We observe differences in detail: 1mUra$^+$ increases the energy gap between the cation states, while 3mUra$^+$ decreases this gap compared to Ura$^+$, making the cation manifold more compact. Energy and geometry changes are explored in depth below.

We only show top views of the critical structures characterised throughout this study, as the most prominent changes occur in-plane. Nevertheless, it is important to note that $(^2\pi_{H-1}^+/^2n_O^+)_{CI}$ in Ura$^+$ and the effective 3-state conical intersection in 3mUra$^+$ have noticeable out-of-plane ring puckering motions, the latter being displayed in the ESI (Figure S1).

3.2.1 1mUra$^+$

Upon initial photoionisation assumed to the $^2\pi_{H-1}^+$ state, 1mUra$^+$ (Fig. 4a) presents a downwards relaxation pathway to the $(^2\pi_{H-1}^+/^2n_O^+)_{CI}$ conical intersection, which is placed 1.12 eV adiabatically above the reference $(^2\pi_H^+)_{min}$. This conical intersection also features an energy gap with the $^2\pi_H^+$ state of 0.35 eV, smaller than that for Ura$^+$ (0.50 eV) and 5mUra$^+$ (0.46 eV). Upon reaching this conical intersection, population will be rapidly funnelled down to the $^2n_O^+$ state. This initial decay leads to pronounced elongation of C2-N3 and N3-C4 bonds with respect to the starting FC region.

On the $^2n_O^+$ state, relaxation continues towards $(^2n_O^+)_{min}$ with a pronounced (0.07 Å) C4-O elongation and an even more marked 0.16 Å N3-C4 bond shortening. $(^2n_O^+)_{min}$ is placed adiabatically at 0.53 eV and is separated from the cation ground state by 0.16 eV at this geometry. There is then a very small (0.03 eV) energy barrier to reach the $(^2n_O^+/^2\pi_H^+)_{CI}$ that mediates population transfer

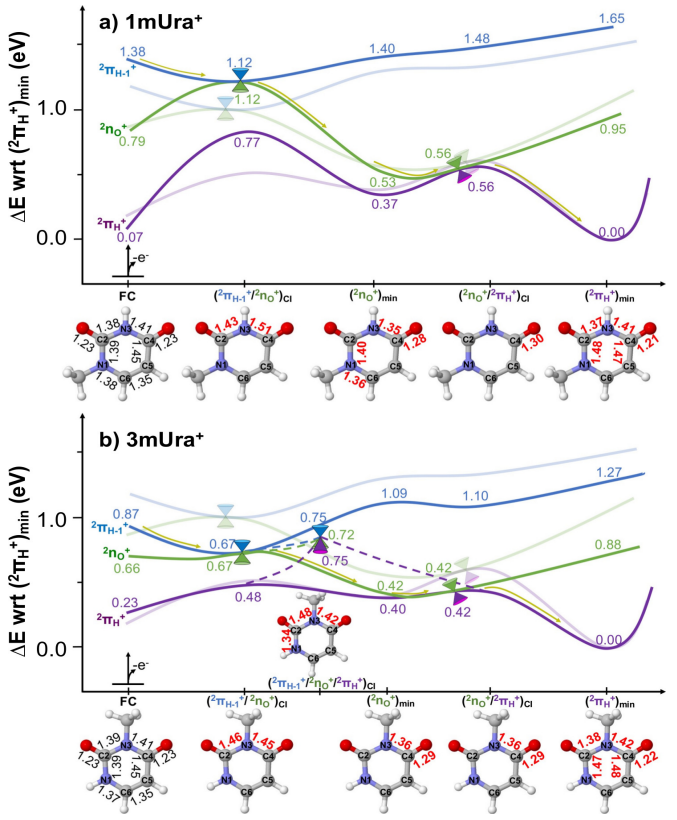

Fig. 4 Potential energy surfaces of a) 1mUra$^+$ and b) 3mUra$^+$ computed at the XMS-CASPT2(IPEA=0.0) level of theory. All energies are given in eV with respect to $(^2\pi_H{}^+)_{min}$, on the right (not FC / the S_0 minimum, as in Fig. 3). Dark yellow arrows represent the evolution of the excited state population starting from the highest-lying $^2\pi^+_{H-1}$ state. XMS-CASPT2 optimised structures are provided with the main bond length changes from FC (in Å) given in red. The 3-state conical intersection decay channel in 3mUra$^+$ is also included in dashed lines. The potential energy surfaces of Ura$^+$ [17] are provided in faded colours as a reference.

down to the $^2\pi^+_H$ cation ground state.

Once population funnels down to $^2\pi^+_H$, final relaxation towards $(^2\pi^+_H)_{min}$ leads to C4-O as well as C2-N3 and N3-C4 bond lengths recovering S_0 minimum-like distances of 1.21, 1.38 and 1.42 Å, respectively, while a pronounced elongation of 0.08 Å in the N1-C2 bond remains.

We expect 1mUra$^+$ to feature a barrierless and rapid $^2\pi^+_{H-1} \rightarrow {}^2n^+_O \rightarrow {}^2\pi^+_H$ step-wise decay similar to that of Ura$^+$ based on XMS-CASPT2 calculations.[17] Cation excited state decay in 1mUra$^+$ is therefore expected to be ultrafast, as in Ura$^+$.[17,35,68]

3.2.2 3mUra$^+$

3mUra$^+$, on the other hand, shows a more closely spaced cationic state manifold (Fig. 4b): three states within a 0.7 eV range in the FC region compared to Ura$^+$. We again consider initial population of the highest-lying cationic state $^2\pi^+_{H-1}$ calculated here.

As discussed in Section 3.1, 3mUra$^+$ presents almost degenerate $^2\pi^+_{H-1}$ and $^2n^+_O$ states, which already suggests the presence of a crossing close to the FC region. Relaxing to this $(^2\pi^+_{H-1}/{}^2n^+_O)_{CI}$ structure leads to bond stretches of around 0.05 Å for the C2-N3 and N3-C4 bonds. Additionally, this intersection features an energy gap of less than 0.2 eV to the cation ground state $^2\pi^+_H$. This conical intersection otherwise resembles those obtained for 1mUra$^+$ and for Ura$^+$ and 5mUra$^+$.[17]

Further optimisation from $(^2\pi^+_{H-1}/{}^2n^+_O)_{CI}$ led to an effective 3-state conical intersection (slightly non-planar, depicted in the supplementary information Fig. S1). This crossing is placed 0.75 eV adiabatically above $(^2\pi^+_H)_{min}$, but it is nevertheless energetically accessible following initial population of the $^2\pi^+_{H-1}$ state (0.87 eV, Fig. 4b). This type of intersection was suggested for Ura$^+$ in the literature[35,36,72] but was questioned, as including dynamic electron correlation increases the energy gap to ~0.5 eV in this prototypical case.[17] However, 3-methylation significantly reduces this energy gap and an effective 3-state crossing could be located. This means a direct $^2\pi^+_{H-1} \rightarrow {}^2\pi^+_H$ decay channel potentially operates for 3mUra$^+$.

Upon crossing at $(^2\pi^+_{H-1}/{}^2n^+_O)_{CI}$, population relaxes further to $(^2n^+_O)_{min}$. This minimum is characterised by a pronounced elongation (0.06 Å) of the C4-O carbonyl bond and a 0.09 Å N3-C4 bond shortening. Energetically this minimum is placed 0.42 eV adiabatically above $(^2\pi^+_H)_{min}$; separated by only 0.02 eV from the $^2\pi^+_H$ state at this geometry. Given the very small energy difference between states in the region of $(^2n^+_O)_{min}$, it is clear that this structure is very close to $(^2n^+_O/{}^2\pi^+_H)_{CI}$, and access to this crossing is essentially barrierless. $(^2n^+_O/{}^2\pi^+_H)_{CI}$ is also structurally almost identical to $(^2n^+_O)_{min}$ except for a very small C1-N2 bond shortening of 0.01 Å. Upon reaching the intersection, population is expected to be funnelled to the cation $^2\pi^+_H$ ground state and to relax to its minimum $(^2\pi^+_H)_{min}$, leading to further pronounced N1-C2, N3-C4 and C4-C5 bond elongations of 0.08, 0.06 and 0.05 Å, respectively, together C2-N3 and C4-O bond shortenings of 0.05 and 0.06 Å. As with 1mUra$^+$ the overall change from the S_0 minimum starting point is the elongation of the N1-C2 bond.

Methylation at the 3' position involves more pronounced changes in the processes following photoionisation than those introduced when substituting at 1'. This can be rationalised as the methyl group is substituted at the part of the molecular frame where both $^2n^+_O$ and $^2\pi^+_{H-1}$ SOMOs are localised; the methyl group has an inductive electron donor effect that impacts more prominently these two states by stabilising them and making them almost degenerate in energy at the equilibrium FC region. Decay of 3mUra$^+$ is also expected to be ultrafast, much like 1mUra$^+$, Ura$^+$ and 5mUra$^+$.[17]

Summarising, we expect 3mUra$^+$ to decay barrierlessly from the initially accessed $^2\pi^+_{H-1}$ state through either $(^2\pi^+_{H-1}/{}^2n^+_O)_{CI}$ or the effective 3-state conical intersection, both of which are energetically accessible. This suggests a competition between a step-wise $^2\pi^+_{H-1} \rightarrow {}^2n^+_O \rightarrow {}^2\pi^+_H$ and a direct $^2\pi^+_{H-1} \rightarrow {}^2\pi^+_H$ decay, which is different from the other uracil systems compared here.

3.3 Methylation effects on conical intersection topographies

Conical intersections control excited state decay depending on their accessibility and topography/shape.[73–78]

To compare the topography of the optimised conical intersections we follow the procedure described by Fdez Galván et al[65] to obtain estimates for pitch (δ), asymmetry (Δ), relative tilt (σ),

Table 1 Conical intersection parameters[65] for the different crossings found in Ura^+, $1mUra^+$, $3mUra^+$ and $5mUra^+$ at the XMS-CASPT2 level of theory. Pitch (δ), asymmetry (Δ) and relative tilt (σ) are given in atomic units, whereas tilt headings (θ_s) are in degrees.

	δ	Δ	σ	θ_s	$\mathscr{P}$	$\mathscr{B}$	Intersection Type[65]
$(^2n_O^+/^2\pi_H^+)_{CI}$							
Ura^+	0.043	0.882	1.326	0.003	0.934	1.021	Peaked, single-path
$1mUra^+$	0.039	0.886	2.380	0.022	3.002	1.507	Sloped, single-path
$3mUra^+$	0.043	0.872	5.577	0.005	16.612	2.677	Sloped, single-path
$5mUra^+$	0.044	0.872	3.089	0.036	5.097	1.809	Sloped, single-path
$(^2\pi_{H-1}^+/^2n_O^+)_{CI}$							
Ura^+	0.051	0.592	1.154	43.164	1.972	1.496	Sloped, single-path
$1mUra^+$	0.034	0.456	2.410	1.967	3.998	1.414	Sloped, single-path
$3mUra^+$	0.050	0.875	0.533	3.055	0.157	0.590	Peaked, bifurcating
$5mUra^+$	0.052	0.940	1.798	5.402	2.131	1.285	Sloped, single-path

and tilt heading (θ_s). These values are used to classify crossing topographies as peaked or sloped, and bifurcating or single-path, based on the $\mathscr{P}$ and $\mathscr{B}$ values defined by Fdez Galván et al.,[65] which resemble those previously proposed by Ruedenberg and co-workers in their seminal work on conical intersection characterisation.[79] Values of $\mathscr{P} < 1$ lead to peaked topographies and > 1 to sloped ones, whereas $\mathscr{B} < 1$ refers to bifurcating character and > 1 to single-path.[65] Table 1 shows the conical intersections parameters for the different species characterised in this work.

Starting with $(^2\pi_{H-1}^+/^2n_O^+)_{CI}$, we predict a sloped and single-path character for all systems except $3mUra^+$, which displays a strong peaked and bifurcating character. We suspect the character of this crossing for $3mUra^+$ relates to the nearby effective 3-state conical intersection at slightly higher energy (see Section 3.2.2).

The $(^2n_O^+/^2\pi_H^+)_{CI}$ presents smaller differences, indicating a sloped and single-path character for all systems studied with the exception of Ura^+, which however features a $\mathscr{P}$ value of 0.934 very close to the threshold to be considered sloped. Sloped single-path intersections have been suggested to underpin photostability,[80,81] as the decay path aligns with the direction towards the formation/recovery of the reactant (cationic) ground state. All intersections are planar, as seen by the $\sim$0 estimates of the tilt heading, which confirms what the potential energy surfaces explored above suggests: methylation does not significantly impact this particular final step of the decay.

3.4 Dynamic electron correlation and its role in photoionisation decay

We investigate the changes to energies and geometries that arise from including dynamic electron correlation while maintaining a description of static electron correlation effects, which are mandatory to adequately describe non-adiabatic processes,[82–84] particularly those between excited and ground electronic states.[85,86] To do this we re-optimised all critical structures located for the different uracil species with CASSCF (Fig. 5) and compared them to those obtained at the XMS-CASPT2 level of theory (Fig. 4) with the same orbital active space.

Fig. 5 shows the superimposed potential energy surfaces with CASSCF (dashed lines) and XMS-CASPT2 (full lines) levels of theory for a) $1mUra^+$ and b) $3mUra^+$, the respective curves for Ura^+ and $5mUra^+$ having been reported and discussed elsewhere.[17]

Fig. 5a shows how $1mUra^+$ displays parallel surfaces with CASSCF and XMS-CASPT2, which lead to qualitatively analogous decays. We see the spread of energies is much greater with CASSCF compared to XMS-CASPT2, and in particular the energy gap between $(^2\pi_{H-1}^+/^2n_O^+)_{CI}$ and the $^2\pi_H^+$ ground state almost doubles if dynamic correlation is not included (0.35 eV with XMS-CASPT2 *vs* 0.66 eV with CASSCF).

For $3mUra^+$ (Fig. 5b) the range of cation state energies is also larger with CASSCF compared to XMS-CASPT2. However, CASSCF also places $^2\pi_{H-1}^+$ and $^2n_O^+$ states very close together in energy in the FC region, although the energy gap between $(^2\pi_{H-1}^+/^2n_O^+)_{CI}$ and $^2\pi_H^+$ still increases (0.19 eV with XMS-CASPT2 *vs* 0.32 eV with CASSCF).

We find two qualitative differences between CASSCF and XMS-CASPT2 for $3mUra^+$. We could not find a CASSCF $(^2n_O^+)_{min}$ structure. This is consistent with the fact that we found the nearby $(^2n_O^+/^2\pi_H^+)_{CI}$ to be peaked and single-path (see Table S3) with CASSCF in this case instead of sloped.

The other very distinctive change with CASSCF for $3mUra^+$ is in the reaction coordinate mediating passage through $(^2n_O^+/^2\pi_H^+)_{CI}$. We observe a symmetric stretching of C2-N3 and N3-C4 bonds, which delocalises geometrical distortions over both carbonyl groups, leading to modest elongation along C4=O as opposed to the localised stretch obtained with XMS-CASPT2 (1.23 Å *vs* 1.29 Å, for CASSCF and XMS-CASPT2, respectively).

In summary, dynamic electron correlation has a quantitative effect for $1mUra^+$ but a qualitative effect for $3mUra^+$.

4 Conclusions

In this article we explore how methylation alters the excited state decay processes in photoionised uracil using multireference XMS-CASPT2 methods. To do this we present new data on 1- and 3-methylated uracil, and compare against previously published results[17] for uracil and 5-methylated uracil (thymine).

Methylation does not change the ordering of the cation electronic states for the four systems compared here.

Within this framework, we find that 3-methylation leads to distinctive changes: initially by reducing the energy gaps between the first three cation states, with almost degenerate $^2\pi_{H-1}^+$ and $^2n_O^+$ states at the S_0 minimum geometry in this case.

Upon populating the $^2\pi_{H-1}^+$ state, we first expect rapid decay to the $^2n_O^+$ state through an accessible $^2\pi_{H-1}^+/^2n_O^+$ conical intersection. This $^2\pi_{H-1}^+/^2n_O^+$ intersection in $3mUra^+$ also features a

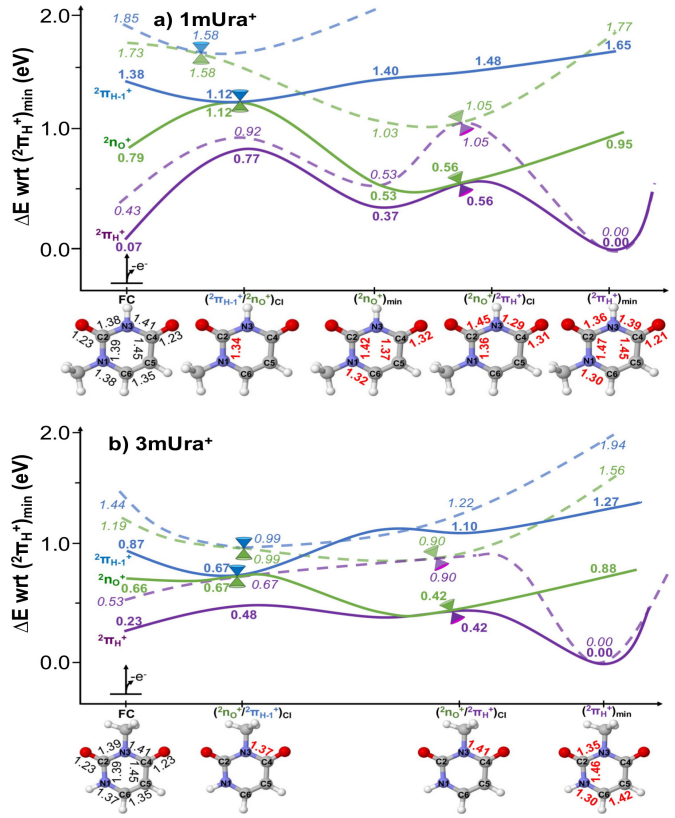

Fig. 5 Potential energy surfaces of a) 1mUra$^+$ and b) 3mUra$^+$ computed at the CASSCF level of theory (dashed lines) compared with the XMS-CASPT2 reference (full lines, from Fig. 4). All energies are given in eV with respect to $(^2\pi_H)_{min}$ on the right (not FC): bold values for XMS-CASPT2 italics referring to CASSCF. CASSCF optimised structures are also provided, with main bond length changes (in Å) given in red.

small (< 0.2 eV) energy gap to the $^2\pi_H^+$ cation ground state and a peaked, bifurcating topography. Upon further optimisation we located an effective 3-state conical intersection which lies ∼0.1 eV higher in energy and is therefore accessible from the initially populated $^2\pi_{H-1}^+$ state.

We predict that 3mUra$^+$ will have the shortest excited state decay lifetime of all methylated and un-methylated systems compared herein: it presents the smallest energy gap between the initially accessed and final states, and it potentially features both direct ($^2\pi_{H-1}^+ \rightarrow {}^2\pi_H^+$, mediated by an effective 3-state CI) and sequential ($^2\pi_{H-1}^+ \rightarrow {}^2n_O^+ \rightarrow {}^2\pi_H^+$) radiationless decay mechanisms. $^2n_O^+ \rightarrow {}^2\pi_H^+$ decay via the conical intersection between these two states is barrierless for 3mUra$^+$.

1mUra$^+$, on the other hand, shows analogous decays to those previously observed for Ura$^+$ and 5mUra$^+$.[17] Methylation slightly red-shifts the on-set of ionisation, as was observed for 5mUra$^+$. 1'-substitution reduces the energy gap between the $^2\pi_{H-1}^+/{}^2n_O^+$ crossing and the cation ground state, but - even at the correlated XMS-CASPT2 level - this gap nevertheless appears to be too large for an effective and accessible 3-state intersection. Decay is consequently expected to occur only sequentially, as was previously suggested for Ura$^+$ and 5mUra$^+$.

Dynamic electron correlation affects the excited state decay process quantitatively for 1mUra$^+$ but qualitatively for 3mUra$^+$. While CASSCF state orderings are unchanged, 3mUra$^+$ shows a different $^2n_O^+/{}^2\pi_H^+$ crossing topography. Additionally, geometric distortions at this crossing are localised on the C4=O bond when using XMS-CASPT2 (as in the other systems compared here) but they delocalise over the two carbonyl groups and surroundings when using CASSCF for 3mUra$^+$, leading to different reaction coordinates mediating decay.

This work deepens our understanding of how potential energy landscapes, as well as the conical intersections connecting them, are affected by chemical substitution (methylation in this case) as well as by the treatment of electron correlation included in the computational model. Methylation in the 3' position alters the behaviour of the RNA base uracil and appears to open an additional pathway for radiationless decay following ionisation and electronic excitation.

Author Contributions

Conceptualization: J.S.-M. Data curation: J.S-M. Funding acquisition: J.S.-M. and M.J.B. Project administration: J.S.-M. and M.J.B. Resources: M.J.B. Investigation: J.S.-M. and T.T. Supervision: J.S.-M. and M.J.B. Validation & Visualization: J.S.-M. and T.T. Writing – original draft: J.S.-M. Writing – review editing: J.S.-M., T.T. and M.J.B.

Conflicts of interest

There are no conflicts to declare.

Acknowledgements

Prior support from the European Commission through the Marie Curie actions (*AttoDNA*, FP8-MSCA-IF, grant nº 747662) is acknowledged. The project that gave rise to these results received the support of a fellowship from "La Caixa" Foundation (ID 100010434) and from the European Union's Horizon 2020 research and innovation programme under the Marie Skłodowska-Curie grant agreement No 847648, fellowship code "LCF/BQ/PI20/11760022" (J. S.-M.). We gratefully acknowledge the computational resources and support provided by the Imperial College Research Computing Service (DOI: 10.14469/hpc/2232). J.S.-M. acknowledges computing resources from *Tirant III* and technical support provided by the *Servei d'Informatica de la Universitat de Valencia*.

Notes and references

1 C. T. Middleton, K. de La Harpe, C. Su, Y. K. Law, C. E. Crespo-Hernández and B. Kohler, *Annual Review of Physical Chemistry*, 2009, **60**, 217–239.

2 C. E. Crespo-Hernández, B. Cohen, P. M. Hare and B. Kohler, *Chem. Rev.*, 2004, **104**, 1977–2020.

3 S. Boldissar and M. S. de Vries, *Phys. Chem. Chem. Phys.*, 2018, **20**, 9701–9716.

4 A. A. Beckstead, Y. Zhang, M. S. de Vries and B. Kohler, *Phys. Chem. Chem. Phys.*, 2016, **18**, 24228–24238.

5 W. J. Schreier, P. Gilch and W. Zinth, *Annual Review of Physical Chemistry*, 2015, **66**, 497–519.

6 F. P. Noonan, M. R. Zaidi, A. Wolnicka-Glubisz, M. R. Anver,

J. Bahn, A. Wielgus, J. Cadet, T. Douki, S. Mouret, M. A. Tucker, A. Popratiloff, G. Merlino and E. C. De Fabo, *Nature Communications*, 2012, **3**, 884.

7 T. Gustavsson, Bányász, E. Lazzarotto, D. Markovitsi, G. Scalmani, M. J. Frisch, V. Barone and R. Improta, *Journal of the American Chemical Society*, 2006, **128**, 607–619.

8 L. Martínez-Fernández, A. J. Pepino, J. Segarra-Martí, A. Banyasz, M. Garavelli and R. Improta, *Journal of Chemical Theory and Computation*, 2016, **12**, 4430–4439.

9 L. Martínez-Fernández, A. J. Pepino, J. Segarra-Martí, J. Jovaišaitė, I. Vaya, A. Nenov, D. Markovitsi, T. Gustavsson, A. Banyasz, M. Garavelli and R. Improta, *Journal of the American Chemical Society*, 2017, **139**, 7780–7791.

10 L. Martínez Fernández, F. Santoro and R. Improta, *Accounts of Chemical Research*, 2022, **0**, DOI:10.1021/acs.accounts.2c00256.

11 L. Esposito, A. Banyasz, T. Douki, M. Perron, D. Markovitsi and R. Improta, *Journal of the American Chemical Society*, 2014, **136**, 10838–10841.

12 S.-G. Jin, W. Xiong, X. Wu, L. Yang and G. P. Pfeifer, *Genomics*, 2015, **106**, 322–330.

13 W. J. Schreier, T. E. Schrader, F. O. Koller, P. Gilch, C. E. Crespo-Hernández, V. N. Swaminathan, T. Carell, W. Zinth and B. Kohler, *Science*, 2007, **315**, 625–629.

14 S. Kumar, V. Chinnusamy and T. Mohapatra, *Frontiers in Genetics*, 2018, **9**, 640.

15 A. Breiling and F. Lyko, *Epigenetics & chromatin*, 2015, **8**, 1–9.

16 D. Roca-Sanjuán, M. Rubio, M. Merchán and L. Serrano-Andrés, *The Journal of Chemical Physics*, 2006, **125**, 084302.

17 J. Segarra-Martí, T. Tran and M. J. Bearpark, *Phys. Chem. Chem. Phys.*, 2019, **21**, 14322–14330.

18 J. Segarra-Martí, T. Tran and M. J. Bearpark, *ChemPhotoChem*, 2019, **3**, 856–865.

19 D. Dougherty, K. Wittel, J. Meeks and S. P. McGlynn, *Journal of the American Chemical Society*, 1976, **98**, 3815–3820.

20 G. Lauer, W. Schäfer and A. Schweig, *Tetrahedron Letters*, 1975, **16**, 3939 – 3942.

21 S. Urano, X. Yang and P. R. LeBreton, *Journal of Molecular Structure*, 1989, **214**, 315 – 328.

22 K. D. Fulfer, D. Hardy, A. A. Aguilar and E. D. Poliakoff, *The Journal of Chemical Physics*, 2015, **142**, 224310.

23 J. Segarra-Martí and M. J. Bearpark, *ChemPhysChem*, 2021, **22**, 2172–2181.

24 A. P. Schuch, N. C. Moreno, N. J. Schuch, C. F. M. Menck and C. C. M. Garcia, *Free Radical Biology and Medicine*, 2017, **107**, 110–124.

25 A. Banyasz, T. Ketola, L. Martínez-Fernández, R. Improta and D. Markovitsi, *Faraday Discuss.*, 2018, **207**, 181–197.

26 E. Balanikas, A. Banyasz, T. Douki, G. Baldacchino and D. Markovitsi, *Accounts of Chemical Research*, 2020, **53**, 1511–1519.

27 L. Martinez-Fernandez, P. Changenet, A. Banyasz, T. Gustavsson, D. Markovitsi and R. Improta, *The Journal of Physical Chemistry Letters*, 2019, **10**, 6873–6877.

28 D. B. Bucher, B. M. Pilles, T. Carell and W. Zinth, *Proceedings of the National Academy of Sciences*, 2014, **111**, 4369–4374.

29 I. Vayá, T. Gustavsson, F.-A. Miannay, T. Douki and D. Markovitsi, *Journal of the American Chemical Society*, 2010, **132**, 11834–11835.

30 T. Takaya, C. Su, K. de La Harpe, C. E. Crespo-Hernández and B. Kohler, *Proceedings of the National Academy of Sciences*, 2008, **105**, 10285–10290.

31 M. Nisoli, P. Decleva, F. Calegari, A. Palacios and F. Martín, *Chemical Reviews*, 2017, **117**, 10760–10825.

32 F. Calegari, A. Trabattoni, A. Palacios, D. Ayuso, M. C. Castrovilli, J. B. Greenwood, P. Decleva, F. Martín and M. Nisoli, *Journal of Physics B: Atomic, Molecular and Optical Physics*, 2016, **49**, 142001.

33 T. J. A. Wolf, F. Holzmeier, I. Wagner, N. Berrah, C. Bostedt, J. Bozek, P. Bucksbaum, R. Coffee, J. Cryan, J. Farrell, R. Feifel, T. J. Martinez, B. McFarland, M. Mucke, S. Nandi, F. Tarantelli, I. Fischer and M. Gühr, *Applied Sciences*, 2017, **7**, 681.

34 T. J. A. Wolf and M. Gühr, *Philosophical Transactions of the Royal Society A: Mathematical, Physical and Engineering Sciences*, 2019, **377**, 20170473.

35 M. Assmann, T. Weinacht and S. Matsika, *The Journal of Chemical Physics*, 2016, **144**, 034301.

36 P. Vindel-Zandbergen, S. Matsika and N. T. Maitra, *The Journal of Physical Chemistry Letters*, 2022, **13**, 1785–1790.

37 K. Andersson, P. A. Malmqvist, B. O. Roos, A. J. Sadlej and K. Wolinski, *J. Phys. Chem.*, 1990, **94**, 5483–5488.

38 K. Andersson, P.-Å. Malmqvist and B. O. Roos, *J. Chem. Phys.*, 1992, **96**, 1218–1226.

39 D. Roca-Sanjuán, F. Aquilante and R. Lindh, *WIRES Comput. Mol. Sci.*, 2012, **2**, 585–603.

40 N. Forsberg and P.-Å. Malmqvist, *Chem. Phys. Lett.*, 1997, **274**, 196 – 204.

41 G. Ghigo, B. O. Roos and P.-Å. Malmqvist, *Chem. Phys. Lett.*, 2004, **396**, 142 – 149.

42 J. Finley, P.-Å. Malmqvist, B. O. Roos and L. Serrano-Andrés, *Chem. Phys. Lett.*, 1998, **288**, 299 – 306.

43 A. A. Granovsky, *J. Chem. Phys.*, 2011, **134**, 214113.

44 I. Fdez. Galván, M. Vacher, A. Alavi, C. Angeli, F. Aquilante, J. Autschbach, J. J. Bao, S. I. Bokarev, N. A. Bogdanov, R. K. Carlson, L. F. Chibotaru, J. Creutzberg, N. Dattani, M. G. Delcey, S. S. Dong, A. Dreuw, L. Freitag, L. M. Frutos, L. Gagliardi, F. Gendron, A. Giussani, L. González, G. Grell, M. Guo, C. E. Hoyer, M. Johansson, S. Keller, S. Knecht, G. Kovačević, E. Källman, G. Li Manni, M. Lundberg, Y. Ma, S. Mai, J. P. Malhado, P. Malmqvist, P. Marquetand, S. A. Mewes, J. Norell, M. Olivucci, M. Oppel, Q. M. Phung, K. Pierloot, F. Plasser, M. Reiher, A. M. Sand, I. Schapiro, P. Sharma, C. J. Stein, L. K. Sørensen, D. G. Truhlar, M. Ugandi, L. Ungur, A. Valentini, S. Vancoillie, V. Veryazov, O. Weser, T. A. Wesołowski, P.-O. Widmark, S. Wouters, A. Zech, J. P. Zobel and R. Lindh, *Journal of Chemical Theory and Computation*, 2019, **15**, 5925–5964.

45 F. Aquilante, J. Autschbach, A. Baiardi, S. Battaglia, V. A. Borin, L. F. Chibotaru, I. Conti, L. De Vico, M. Delcey, I. Fdez. Galván, N. Ferré, L. Freitag, M. Garavelli, X. Gong, S. Knecht, E. D. Larsson, R. Lindh, M. Lundberg, P. Malmqvist, A. Nenov, J. Norell, M. Odelius, M. Olivucci, T. B. Pedersen, L. Pedraza-González, Q. M. Phung, K. Pierloot, M. Reiher, I. Schapiro, J. Segarra-Martí, F. Segatta, L. Seijo, S. Sen, D.-C. Sergentu, C. J. Stein, L. Ungur, M. Vacher, A. Valentini and V. Veryazov, *The Journal of Chemical Physics*, 2020, **152**, 214117.

46 T. Shiozaki, C. Woywod and H.-J. Werner, *Phys. Chem. Chem. Phys.*, 2013, **15**, 262–269.

47 S. Sen and I. Schapiro, *Molecular Physics*, 2018, **116**, 2571–2582.

48 T. Shiozaki, *Wiley Interdisciplinary Reviews: Computational Molecular Science*, 2018, **8**, e1331.

49 J. W. Park, R. Al-Saadon, M. K. MacLeod, T. Shiozaki and B. Vlaisavljevich, *Chemical Reviews*, 0, **0**, null.

50 T. H. Dunning, *The Journal of Chemical Physics*, 1989, **90**, 1007–1023.

51 J. Segarra-Martí, A. Francés-Monerris, D. Roca-Sanjuán and M. Merchán, *Molecules*, 2016, **21**, 1666.

52 A. J. Pepino, J. Segarra-Martí, A. Nenov, R. Improta and M. Garavelli, *The Journal of Physical Chemistry Letters*, 2017, **8**, 1777–1783.

53 A. J. Pepino, J. Segarra-Martí, A. Nenov, I. Rivalta, R. Improta and M. Garavelli, *Phys. Chem. Chem. Phys.*, 2018, **20**, 6877–6890.

54 V. K. Jaiswal, J. Segarra-Martí, M. Marazzi, E. Zvereva, X. Assfeld, A. Monari, M. Garavelli and I. Rivalta, *Phys. Chem. Chem. Phys.*, 2020, **22**, 15496–15508.

55 M. J. Bearpark, M. A. Robb and H. B. Schlegel, *Chemical Physics Letters*, 1994, **223**, 269 – 274.

56 T. Shiozaki, W. Győrffy, P. Celani and H.-J. Werner, *The Journal of Chemical Physics*, 2011, **135**, 081106.

57 M. K. MacLeod and T. Shiozaki, *The Journal of Chemical Physics*, 2015, **142**, 051103.

58 B. Vlaisavljevich and T. Shiozaki, *Journal of Chemical Theory and Computation*, 2016, **12**, 3781–3787.

59 J. W. Park and T. Shiozaki, *Journal of Chemical Theory and Computation*, 2017, **13**, 3676–3683.

60 J. W. Park and T. Shiozaki, *Journal of Chemical Theory and Computation*, 2017, **13**, 2561–2570.

61 J. W. Park, R. Al-Saadon, N. E. Strand and T. Shiozaki, *Journal of Chemical Theory and Computation*, 2019, **15**, 4088–4098.

62 S. Matsika and D. R. Yarkony, *Journal of the American Chemical Society*, 2003, **125**, 10672–10676.

63 S. Matsika, *The Journal of Physical Chemistry A*, 2005, **109**, 7538–7545.

64 J. Segarra-Martí, S. M. Nouri and M. J. Bearpark, *Photochem*, 2021, **1**, 287–301.

65 I. Fdez. Galván, M. G. Delcey, T. B. Pedersen, F. Aquilante and R. Lindh, *Journal of Chemical Theory and Computation*, 2016, **12**, 3636–3653.

66 B. I. Verkin, L. F. Sukodub and I. K. Yanson, *Dokl. Akad. Nauk SSSR*, 1976, **228**, 1452.

67 M. Kotur, C. Zhou, S. Matsika, S. Patchkovskii, M. Spanner and T. C. Weinacht, *Phys. Rev. Lett.*, 2012, **109**, 203007.

68 M. Assmann, H. Köppel and S. Matsika, *The Journal of Physical Chemistry A*, 2015, **119**, 866–875.

69 M. Kotur, T. Weinacht, C. Zhou and S. Matsika, *IEEE Journal of Selected Topics in Quantum Electronics*, 2012, **18**, 187–194.

70 M. Kotur, T. C. Weinacht, C. Zhou and S. Matsika, *Phys. Rev. X*, 2011, **1**, 021010.

71 M. Kotur, T. C. Weinacht, C. Zhou, K. A. Kistler and S. Matsika, *The Journal of Chemical Physics*, 2011, **134**, 184309.

72 S. Matsika, *Chemical Physics*, 2008, **349**, 356 – 362.

73 C. A. Farfan and D. B. Turner, *Phys. Chem. Chem. Phys.*, 2020, **22**, 20265–20283.

74 J. P. Malhado, M. J. Bearpark and J. T. Hynes, *Frontiers in Chemistry*, 2014, **2**, 97.

75 M. Vacher, J. Meisner, D. Mendive-Tapia, M. J. Bearpark and M. A. Robb, *The Journal of Physical Chemistry A*, 2015, **119**, 5165–5172.

76 D. R. Yarkony, *Rev. Mod. Phys.*, 1996, **68**, 985–1013.

77 M. Ben-Nun, F. Molnar, K. Schulten and T. J. Martínez, *Proceedings of the National Academy of Sciences*, 2002, **99**, 1769–1773.

78 B. Mignolet, B. F. E. Curchod and T. J. Martínez, *Angewandte Chemie International Edition*, 2016, **55**, 14993–14996.

79 G. J. Atchity, S. S. Xantheas and K. Ruedenberg, *The Journal of Chemical Physics*, 1991, **95**, 1862–1876.

80 K. F. Hall, M. Boggio-Pasqua, M. J. Bearpark and M. A. Robb, *The Journal of Physical Chemistry A*, 2006, **110**, 13591–13599.

81 A. M. Tokmachev, M. Boggio-Pasqua, M. J. Bearpark and M. A. Robb, *The Journal of Physical Chemistry A*, 2008, **112**, 10881–10886.

82 M. Araújo, B. Lasorne, A. L. Magalhães, G. A. Worth, M. J. Bearpark and M. A. Robb, *The Journal of Chemical Physics*, 2009, **131**, 144301.

83 J. J. Serrano-Pérez, F. de Vleeschouwer, F. de Proft, D. Mendive-Tapia, M. J. Bearpark and M. A. Robb, *The Journal of Organic Chemistry*, 2013, **78**, 1874–1886.

84 F. Bernardi, M. Olivucci and M. A. Robb, *Chem. Soc. Rev.*, 1996, **25**, 321–328.

85 R. Crespo-Otero and M. Barbatti, *Chemical Reviews*, 2018, **118**, 7026–7068.

86 M. Barbatti and R. Crespo-Otero, in *Surface Hopping Dynamics with DFT Excited States*, ed. N. Ferré, M. Filatov and M. Huix-Rotllant, Springer International Publishing, Cham, 2016, pp. 415–444.